sequences have been studied extensively and they have many interesting applications in X-ray crystallography, radar codes, convolutional codes, time-hopping communication networks, and also in graph theory.[2,3] However, the general $B_h(n)$ sequences for $h \geq 3$ are more of number theoretic nature and they are relatively less well-known. Some $B_3(n)$ sequences are recently tabulated in Reference 1 and they can be used in carrier frequency assignments for nonlinear repeaters in radio systems.

$B_h(n)$ sequences can be generated by difference sets and hence an optimal $B_h(n)$ sequence has length $l_h^*(n) < n^h$ whenever n is a prime power.[6] By shifting and truncating a difference set, many $B_h(s)$ sequences can be obtained for $s < n$, n being a prime power. The lengths $l_2^*(n)$ of optimal $B_2(n)$ sequences are known for $n \leq 15$, and suboptimal $B_2(n)$ sequences for $n \leq 150$ have been constructed from difference sets.[1,5]

Suppose $a_0 = 0$ in a $B_h(n)$ sequence, then all the h-fold, $(h-1)$-fold, ..., 2-fold, 1-fold sums of nonzero terms in the sequence are distinct and there are exactly $\binom{n-1+h}{h} - 1$ of them. The largest of these distinct positive sums is $hl_h(n)$ and therefore an optimal $B_h(n)$ sequence must have length

$$l_h^*(n) \geq \frac{1}{h}\left[\binom{n-1+h}{h} - 1\right] \quad (3)$$

For $h = 2$, the lower bound can be improved as $l_2^*(n) \geq \max\{(n/2), n^2 - 2n^{1.5}\}$.[1,8] Since a $B_h(n)$ sequence is also a $B_{h-1}(n)$ sequence, it is true that $l_2^*(n) \leq l_3^*(n) \leq \ldots \leq l_h^*(n)$.

Table 1 OPTIMAL $B_h(n)$ SEQUENCES

h	n	Optimal sequences	Difference set sequences
3	3	0, 1, **4**	0, 1, **4**
	4	0, 1, 7, **11**	0, 1, 8, **11**
		0, 1, 8, **11**	
	5	0, 1, 15, 18, **23**	0, 1, 7, 16, **27**
		0, 1, 15, 20, **23**	
	6	0, 2, 11, 26, 42, **45**	0, 14, 18, 45, 51, **56**
	7	0, 1, 7, 50, 59, 78, **82**	0, 52, 73, 97, 106, 114, **120**
		0, 6, 7, 50, 59, 78, **82**	
		0, 2, 23, 45, 72, 79, **82**	
4	4	0, 1, 11, **15**	
		0, 2, 12, **15**	
	5	0, 1, 24, 37, **41**	
	6	0, 1, 17, 70, 95, **100**	
5	5	0, 1, 16, 66, **72**	

It can be shown that $l_2^*(n) < n^2$ whenever $n+1$, n, $n-1$, or $n-2$ is a prime power.[5] In general, the exact values of $l_h^*(n)$ are very difficult to determine and it is not clear that $l_h^*(n)$ is less than n^h for all n. Let $d_1 < d_2 < \ldots < d_{n-1}$ denote a set of $n-1$ distinct positive differences so that $d_1 + d_2 + \ldots + d_{n-1} = l_h(n)$. There are roughly $[l_h(n)]^{n-2}/(n-2)!(n-1)!$ ways of partitioning $l_h(n)$ into $n-1$ distinct parts.[4] For each permutation of a partition, say $l_h(n) = b_1 + b_2 + \ldots + b_{n-1}$, one can generate the sequence $0, b_1, b_1 + b_2, \ldots, b_1 + b_2 + \ldots + b_{n-1}$ and check the $\binom{n-1+h}{h}$ h-sums to see if the sequence is a legitimate $B_h(n)$ sequence. Presuming $l_h(n) \approx n^h$ and using the Stirling approximation for $n!$, it can be shown that the complexity of searching for an optimal $B_h(n)$ sequence is $O(n^{(h-1)n}e^n)$, a formidable task for large values of n.

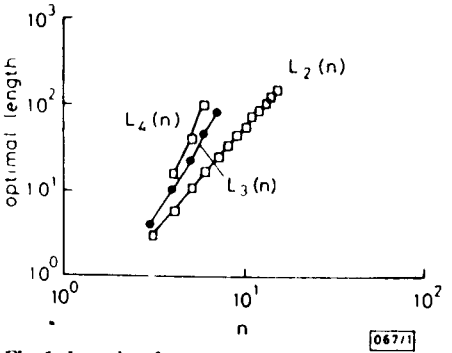

Fig. 1 *Lengths of optimal $B_h(n)$ sequences*

We conjecture that $l_h^*(n)$ is equal to $n^h - n^{f(h)}$, where $f(h)$ is a magic number determined by h. We have found in Reference 5 that $f(2) \approx 1.632$, and our preliminary results on optimal $B_3(n)$ and $B_4(n)$ sequences suggest that $f(3) \approx 2.864$ and $f(4) \approx 3.956$. Our new results on optimal $B_3(n)$, $B_4(n)$, and $B_5(n)$ sequences are displayed in Table 1. Note that the reverse sequence $a_{n-1} - a_{n-1}, a_{n-1} - a_{n-2}, \ldots, a_{n-1} - a_1, a_{n-1} - a_0$ is also a $B_h(n)$ sequence. Also listed in Table 1 are the difference set $B_3(n)$ sequences given in Reference 1 for comparison. It should be noted that the optimal $B_h(n)$ sequences for $h \geq 5$ are extremely difficult to obtain even for small values of n. Our results also suggest that the optimal sequences can be much shorter than those obtained from different sets. Finally, the known values of $l_h^*(n)$ for $h = 2, 3, 4$ are plotted in Fig. 1.

A. W. LAM
X. DUAN

Department of Electrical & Computer Engineering
University of Massachusetts
Amherst, MA 01002, USA

21st February 1989

References

1 ATKINSON, M. D., SANTORO, N., and URRUTIA, J.: 'Integer sets with distinct sums and differences and carrier frequency assignments for nonlinear repeaters', *IEEE Trans.*, 1986, **COM-34**, (6), pp. 614–617
2 BLOOM, G. S., and GOLOMB, S. W.: 'Numbered complete graphs, unusual rulers, and assorted applications'. Theory and Applications of Graphs in America's Bicentennial Year Int. Conf., Kalamazoo, May 1976, pp. 53–65
3 HALBERSTAM, H., and ROTH, K. F.: 'Sequences' (Springer-Verlag, New York, 1982)
4 HALL, M., JUN.: 'Combinatorial theory' (Blaisdell Publishing Company, Massachusetts, 1967)
5 LAM, A. W., and SARWATE, D. V.: 'On optimum time hopping patterns', *IEEE Trans.*, 1988, **COM-36**, (3), pp. 380–382
6 MAIN, A., and CHOWLA, S.: 'On the B_2-sequences of Sidon'. Proc. Natn. Acad. Sci. India, 1944, sect. A, vol. 14, pp. 3–4
7 ROBINSON, J. P.: 'Optimum Golomb rulers', *IEEE Trans.*, 1979, **C-28**, pp. 943–944
8 TAYLOR, H., and GOLOMB, S. W.: 'Rulers—Part I'. Communication Science Institute Technical Report, #85-05-01, Los Angeles, California, May 1985

390

SPONTANEOUS RELAXATION PROCESSES IN IRRADIATED GERMANOSILICATE OPTICAL FIBRES

Indexing terms: Optical fibres, Nonlinear optics, Relaxation

Many potential applications requiring high-power transmission at short wavelengths are hampered by colour-centre formation. It is perhaps not generally realised that the induced absorption continues to evolve after the laser light is blocked. This relaxation phenomenon is studied in germanosilicate fibres at blue/green wavelengths, and fitted to a three-rate analytical model.

Introduction: Optical fibres frequently exhibit nonlinear transmission at relatively modest blue/green intensity levels. These effects can limit the amount of power delivered through a few metres of single-mode fibre to some hundreds of milliwatts at 488 nm, which has severe implications in applications such as laser Doppler velocimetry and dynamic light scattering.[1]

In a series of recent publications[2,3] we have presented evidence supporting the view that two-photon absorption at around 480 nm lies behind this behaviour. The proposed mechanism is as follows. Two-photon absorption breaks the Si–Ge and Ge–Ge bonds characteristic of oxygen-deficient germanosilicates,[2] releasing electrons (via the reaction $h\nu + \text{Ge–Si} \rightleftharpoons \text{Ge}^{\cdot}\text{Si}^{+} + e^{-}$) with sufficient energy to drift through the glass matrix along networks of interconnected Ge centres (narrow bandgap 'electron pathways'), eventually either recombining or being trapped at other Ge sites to form Ge(1) or Ge(2) colour centres. Optical and spontaneous bleaching release electrons from these traps back into the electron-

pathway, where they are free to get trapped elsewhere. The complex interplay of these processes leads to steady-state colour-centre populations that scale with the optical intensity. This means that the measured loss in the fibre will also reach a steady-state level, since the absorption induced in the glass scales with the colour-centre population.

An intriguing feature of the absorption thus induced is that it does not remain constant once the light is switched off, but continues to rise, eventually approaching a steady-state level. It is the relaxation processes behind this spontaneous evolution of the absorption that we address in this letter.

Experimental procedure and results: In our experiments we monitored the loss in the fibre, during and after exposure to blue/green light from an argon ion laser, using a counter-propagating white-light signal (see Reference 3 for experimental details). The low-intensity white light enabled us to monitor the loss after the laser was blocked, while minimising the disturbance to the colour centres. In each experimental run, a fresh 5 m length of fibre was subjected to laser light excitation at 488 nm, at a chosen intensity for a known length of time.

The results of two experimental runs are given in Fig. 1. In our initial attempts to fit to the measured curves, we discovered that three exponential decay rates were necessary to obtain a good fit, and that once these decay rates were established for a given fibre, good fits could be obtained for that fibre in every other experimental case. This suggested that three different types of traps are operating in the glass, each with its own characteristic trapping and bleaching rates. Hence we modelled the relaxation processes by postulating a constant total population of freed electrons that redistributes itself in the available traps by diffusing through the glass matrix, being captured by empty defect centres and released again by spontaneous phonon-driven processes (i.e. spontaneous thermal colour-centre bleaching).

Mathematical model: Denoting the population densities of the occupied traps by n_1, n_2 and n_3, the population of free (untrapped) electrons will be $n_e = N - (n_1 + n_2 + n_3)$, where N is the total number of electrons in the system and is assumed to be conserved. Calling γ_{ei} the rate of free-electron trapping by defects i, and γ_{ie} the rate of spontaneous release from defect i, the following set of three rate equations may be derived:

$$\begin{bmatrix} \{\gamma - (\gamma_{e1} + \gamma_{1e})\} & \gamma_{e1} & \gamma_{e1} \\ \gamma_{e2} & \{\gamma - (\gamma_{e2} + \gamma_{2e})\} & \gamma_{e2} \\ \gamma_{e3} & \gamma_{e3} & \{\gamma - (\gamma_{e3} + \gamma_{3e})\} \end{bmatrix} \times \begin{bmatrix} n_1/N \\ n_2/N \\ n_3/N \end{bmatrix} = \begin{bmatrix} \gamma_{e1} \\ \gamma_{e2} \\ \gamma_{e3} \end{bmatrix} \quad (1)$$

where d/dt has been replaced by γ. It is mathematically straightforward to solve these equations for arbitrary initial populations $n_1(0)$, $n_2(0)$ and $n_3(0)$. The three characteristic normal-mode decay rates are ${}^1\phi$, ${}^2\gamma$ and ${}^3\gamma$, where the superscript in front of a quantity denotes the mode under consideration.

Discussion: It is known that Ge(1) and Ge(2) centres (so labelled according to the number of next-nearest neighbour Ge atoms) have characteristic absorption bands in the UV. Ge(1) centres are associated with a broad absorption at 281 nm with a tail extending well into the blue, and Ge(2) a narrow peak at 213 nm. It is therefore likely that the loss we measure is due entirely to Ge(1) centres. With the assumption that the experimentally measured loss arises solely from the population n_1, we obtained the fits depicted in Fig. 1 for $\gamma_{1e} = 7{\cdot}5 \times 10^{-5}\,s^{-1}$, $\gamma_{2e} = 3{\cdot}6 \times 10^{-4}\,s^{-1}$, $\gamma_{3e} = 1{\cdot}6 \times 10^{-2}\,s^{-1}$, $\gamma_{e1} = 0{\cdot}12\,s^{-1}$, $\gamma_{e2} = 0{\cdot}34\,s^{-1}$ and $\gamma_{e3} = 5 \times 10^{-4}\,s^{-1}$. The related characteristic model decay rates were $0{\cdot}46\,s^{-1}$, $0{\cdot}016\,s^{-1}$ and $1{\cdot}4 \times 10^{-4}\,s^{-1}$.

The model also predicts the evolution of the other two colour-centre populations n_2 and n_3. The dynamics of all three populations for run (*a*) are depicted in Fig. 2. Immediately after the laser light is blocked, the free electrons rush into Ge(1) and Ge(2) traps, causing an initial surge in loss. At the same time, the electrons trapped at Ge(3) sites are spontaneously released and diffuse to nearby Ge(1) and Ge(2) sites, causing a slow further increase in loss. After n_3 has fallen to a negligible level, n_2 (which was rising) begins to fall as electrons (spontaneously released from Ge(2) sites) diffuse into neighbouring Ge(1) sites. In the very long term (after ~11 h), most electrons end up trapped at Ge(1) centres because they have the slowest spontaneous bleaching rate ($\gamma_{1e} = 7{\cdot}5 \times 10^{-5}\,s^{-1}$).

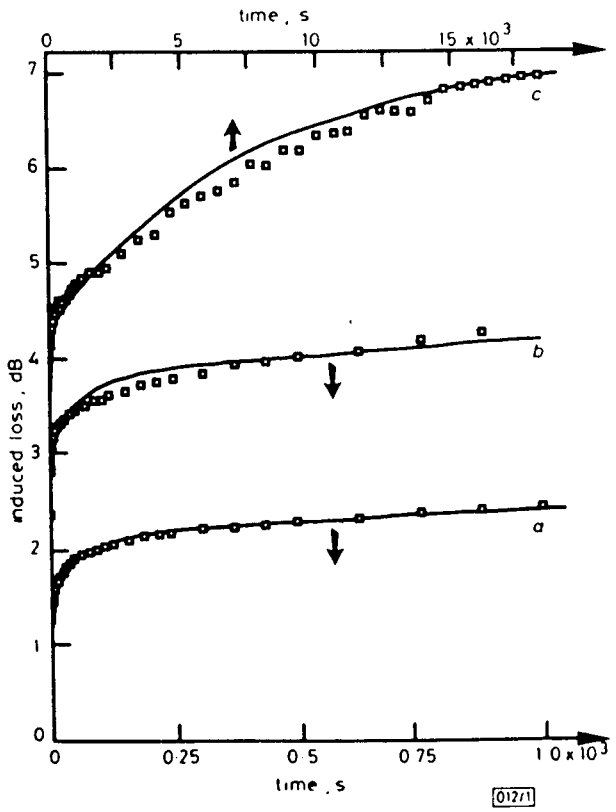

Fig. 1 *Spontaneous increase in loss after exposure to (a) 67 mW/μm², (b) 114 mW/μm² and (c) 125 mW/μm²*

□□□ experimental points ——— theoretical fits

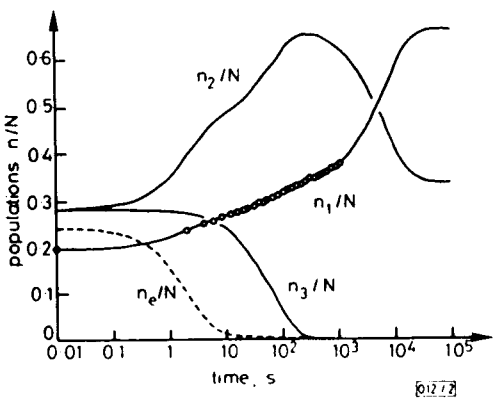

Fig. 2 *Evolution of three colour-centre and free electron populations, together with experimental points for run (a)*

Conclusions: The relaxation processes in germanosilicate optical fibres, after exposure to blue/green light, are dominated by spontaneous trapping and release of electrons to and from three defect species, thought to be Ge(1), Ge(2) and Ge(3) centres. This leads analytically to three characteristic decay rates that agree well with experimental measurements of the evolution of the absorption after exposure to various different optical intensities. Obviously, the relative distributions of Ge(1), Ge(2) and Ge(3) defects will be determined by the germania concentration. This suggests the possibility of designing fibres with optimum relative defect populations for particular applications.

Acknowledgment: This work was funded by the UK Royal Signals & Radar Establishment.

L. J. POYNTZ-WRIGHT

York Limited
York House
School Lane, Chandlers Ford, Hants. SO5 3DG, United Kingdom

P. ST. J. RUSSELL

Optical Fibre Group
Department of Electronics
University of Southampton
Southampton SO9 5NH, United Kingdom

12th December 1988

References

1 BROWN, R. G. W., JACKSON, D. A., JONES, J. D. C., and CHAN, R. K. Y.: 'High power fibre optic laser anemometry'. ICO-13 proc., Sapporo, Japan, Aug. 1984
2 POYNTZ-WRIGHT, L. J., FERMANN, M. E., and RUSSELL, P. ST. J.: 'Nonlinear transmission and colour-centre dynamics in germanosilicate fibres at 420–540 nm', *Opt. Lett.*, 1988, **13**, pp. 1023–1025
3 POYNTZ-WRIGHT, L. J., and RUSSELL, P. ST. J.: 'Photochromic dynamics and nonlinear transmission at modulated CW blue/green wavelengths in germanosilicate optical fibres', *Electron. Lett.*, 1988, **24**, pp. 1054–1055

DISPERSION SENSITIVITY OF INFRA-RED DISPERSION-SHIFTED FIBRES

Indexing terms: Optical fibres, Optical dispersion

Dispersion sensitivity due to small core radius changes for infra-red dispersion-shifted fibres with various α-index profiles is investigated. It is shown that the dispersion sensitivity decreases as α decreases. Moreover, the bending sensitivity is also described and fibre parameters suitable for fully utilising the low intrinsic loss are summarised.

Introduction: Heavy metal fluoride glass (HMF) optical fibres are attractive media for future long-haul and large-capacity transmission systems. HMF optical fibres are predicted to have intrinsic attenuation between 0·001 and 0·01 dB/km with corresponding wavelengths of minimum loss between 2 and 10 μm.[1] To fully utilise the very low intrinsic losses in fibres caused by Rayleigh scattering and absorption, it is essential that the extrinsic losses due to waveguide structures be reduced below the level of intrinsic loss. It is also important to use any available knowledge of system considerations, material properties, and waveguide parameters such as dispersion, and radiation losses due to microbending and macrobending, to guide the choice of appropriate glass materials and fibre fabrication techniques. Until now, there have been few reports on dispersion properties of HMF single-mode fibres having step-index profiles[2] and various α-index profiles.[3] However, the dispersion sensitivity, important in fabricating HMF single-mode fibres, has not been reported on for various α-index profiles.

This letter focuses on the dispersion sensitivity due to small core radius changes and the dispersion slopes around zero-dispersion wavelengths for HMF fibres with various α-index profiles. Moreover, the bending sensitivities of these fibres are also investigated.

Dispersion sensitivity due to a small core radius change: The ZBLA optical fibre consisting of zirconium, barium, lanthanum and aluminium is typical of most zirconium and hafnium based fluoride glasses. It is dealt with here because much of effort has been focused on zirconium fluoride-based glasses. These fibres have a predicted minimum loss of 0·01 dB/km at 2·2 μm. The zero-material-dispersion wavelength of ZBLA is 1·684 μm.[4] Chromatic dispersion is expressed as the sum of the material and waveguide dispersions, i.e.

$$\sigma = \frac{1}{c}\left[k\frac{dN_1}{dk} + n_1\Delta V\frac{d^2(Vb)}{dV^2}\right] \quad (1)$$

where k ($= 2/\lambda$) is wave number and λ is operating wavelength, c represents the light velocity in a vacuum, V is the normalised frequency, b the normalised propagation constant, and Δ the relative index difference. Here n_1 and N_1 are the refractive and group indexes of the core, respectively. The first and second terms on the right-hand side in eqn. 1 represent the material and waveguide dispersions, respectively. The material dispersion can be estimated by the Sellmeiers' coefficients.[4]

Here, the dispersion sensitivity due to a small core radius change $d\sigma/da$ in various α-index fibres ($\alpha = 0{\cdot}5, 1, \infty$) is calculated. Fibre parameters are determined so as to achieve zero dispersion in eqn. 1 at 2·2 μm.

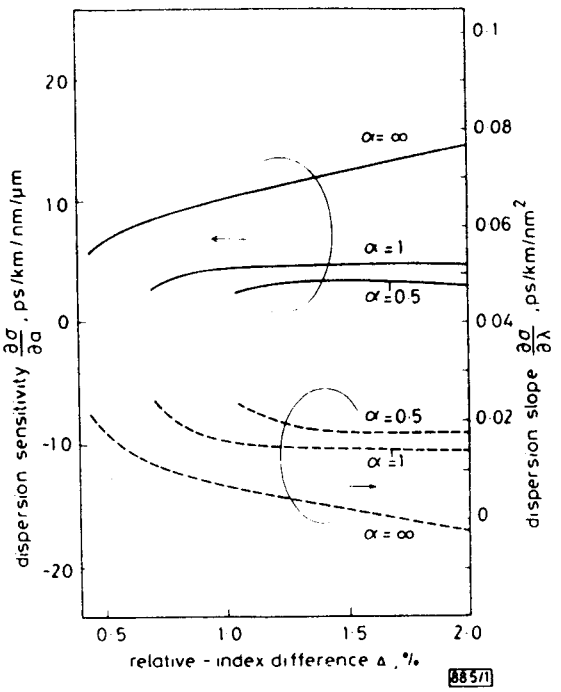

Fig. 1 *Relationship of relative-index difference Δ to dispersion sensitivity dσ/da (solid lines) and Δ to dispersion slope dσ/dλ (broken lines) around zero-dispersion wavelength λ_0*

ZBLA, $\lambda_0 = 2{\cdot}2\,\mu m$

Fig. 1 shows the relationship between the relative-index difference Δ and the dispersion sensitivity $d\sigma/da$. It is found that the dispersion sensitivity increases as the relative index difference Δ or α increase. Dispersion sensitivity is small compared with silica based dispersion-shifted fibres with α-index profiles.[5] This is because the slope of the material dispersion of ZBLA is smaller than that of the silica and the operating wavelength becomes longer. Dispersion slope $d\sigma/d\lambda$ around zero-dispersion wavelengths is shown by broken lines in Fig. 1. It is found that the dispersion slope decreases with increasing relative index difference Δ; the dispersion slope becomes smaller as α increases. For example, the tolerance of the core radius for the step-index fibres with Δ 0·7% is within 0·1 μm to tailor the dispersion at 2·2 μm to within 1 ps/km/nm and the dispersion slope is estimated to be 0·01 ps/km/nm^2. As shown in Fig. 1, it is found that the relationship between the dispersion sensitivity and the dispersion slope is a compromise. Dispersion slope of ZBLA is far smaller than that of silica-based dispersion-shifted fibres.[6] This is also because the material dispersion slope of ZBLA is smaller than that of silica.

At present, the profile of HMF fibres cannot be controlled because of fabrication techniques such as suction casting and rotating casting. However, if a fabrication technique like vapour axial deposition could be developed, the dispersion controllability would be further improved.

Bending property: In designing the fibre parameters, the bending property is an important key factor. Fig. 2 shows the relation between the relative index difference Δ and the allowable bending radius R^* at 2·2 μm. Here, the allowable bending radius R^* is defined as the radius giving the bending loss of 0·001 dB/km at 2·2 μm and corresponds to the bending loss.